

Introducing Augmented Reality to Optical Coherence Tomography in Ophthalmic Microsurgery

Hessam Roodaki*

Technische Universität München

Konstantinos Filippatos†

Carl Zeiss Meditec AG

Abouzar Eslami‡

Carl Zeiss Meditec AG

Nassir Navab§

Technische Universität München
and Johns Hopkins University

ABSTRACT

Augmented Reality (AR) in microscopic surgery has been subject of several studies in the past two decades. Nevertheless, AR has not found its way into everyday microsurgical workflows. The introduction of new surgical microscopes equipped with Optical Coherence Tomography (OCT) enables the surgeons to perform multimodal (optical and OCT) imaging in the operating room. Taking full advantage of such elaborate source of information requires sophisticated intraoperative image fusion, information extraction, guidance and visualization methods. Medical AR is a unique approach to facilitate utilization of multimodal medical imaging devices. Here we propose a novel medical AR solution to the long-known problem of determining the distance between the surgical instrument tip and the underlying tissue in ophthalmic surgery to further pave the way of AR into the surgical theater. Our method brings augmented reality to OCT for the first time by augmenting the surgeon's view of the OCT images with an estimated instrument cross-section shape and distance to the retinal surface using only information from the shadow of the instrument in intraoperative OCT images. We demonstrate the applicability of our method in retinal surgery using a phantom eye and evaluate the accuracy of the augmented information using a micromanipulator.

Keywords: Augmented reality, optical coherence tomography, ophthalmic surgery, instrument cross-section.

Index Terms: H.5.1 [Information Interfaces and Presentation]: Multimedia Information Systems—Artificial, augmented, and virtual realities

1 INTRODUCTION

Ophthalmic posterior segment surgery is a complex manual task performed under a surgical stereo microscope that involves manipulation of delicate retinal tissue. Surgical accuracy required in a microsurgery task is in the scale of tens of micrometers which is at or close to the limit of human positional ability. The interactions between the surgical instrument and the retinal membranes are also below the limit of human tactile sensation. Limited positional and tactile sensation in a vitreoretinal surgery leads to the reliance of the surgeon primarily on the microscopic visual feedback which is known to dramatically reduce the manipulation quality, speed and accuracy [14]. Perceiving depth and instrument-tissue proximity to avoid retinal damage is a challenging burden for the surgeon. For this reason, development of assistive algorithms such as retinal surgery instrument detection or proximity estimation in microscopic images has become a research interest in the computer vision community [13, 18]. Such a task requires real-time

tracking under challenging conditions such as lens distortions, rapid instrument motions, partial occlusions and illumination variations imposed by handheld endo-illumination probe.

Compared to conventional microscopic imaging, Optical Coherence Tomography (OCT) is a fundamentally different imaging modality that has become a major non-invasive tool in ophthalmology. OCT B-scans provide real-time cross-sectional images of retina with resolutions close to that of histopathology and higher than any other non-invasive imaging modality. Diagnosis of chorioretinal diseases and monitoring morphological retinal changes over time using OCT are well-established approaches [5, 6]. Until recently, OCT scanners were available only in tabletop form factors and restricted to the diagnostic setting. Faster image acquisition by Spectral Domain OCT (SD-OCT) led to introduction of handheld OCT scanners. However, their inability to visualize ocular structures in real-time during surgical maneuvers has limited their intraoperative applicability [15]. Since optical microscopy and OCT can share the same optical path in a device, integration of OCT and surgical microscope was a natural next step to address limitations in maneuver, accuracy and speed associated with handheld OCT scanners [11, 20]. Microscope-mounted intraoperative OCT (iOCT) solution by Carl Zeiss Meditec (*RESCAN 700*) with foot pedal control of the OCT and real-time overlay on microscopic view using Heads-Up Display (HUD) has been the first in this category to be described in human use [9, 10].

Integration of OCT into the operating room has a significant impact on surgical decision-making by providing information regarding surgical maneuvers and their effect on tissues [8]. Examples include membrane identification and removal confirmation in Epiretinal Membrane (ERM) peeling procedure [12, 4] and intraoperative measurement of the anterior lens capsule position [16]. Intraoperative application of OCT has also limitations including latency and positional drifts. Also, optical properties of routinely used metallic instruments include high reflectivity resulting in total shadowing and obstructing the view of the underlying tissues in OCT images. By turning a limitation into an opportunity, we present a novel method to use information provided by reflections and shadows of surgical instruments to estimate the instrument cross-section shape and its distance to retina. Providing this extra information helps in perceiving instrument-tissue proximity to avoid unnecessary touch.

The method of choice for the visualization of extra cross-sectional and depth information is a key element of this work. Trials of Augmented Reality (AR) in the operating room show its ability to seamlessly integrate into the surgical workflow [17]. Since vitreoretinal surgery is performed under a surgical microscope, augmenting the surgeon's view with additional information is a reasonable approach. Augmented stereoscopic microscope has already been used both for neuro- and ophthalmo-surgical interventions [3, 7, 19]. Also preliminary use of an overlay system to display preoperative data during a retinal microsurgical intervention has shown to improve the gesture accuracy and reduce the operating time [13]. In this paper, we introduce AR to intraoperative OCT in conventional vitreoretinal microsurgery which to our knowledge is the first of its kind.

*e-mail: he.roodaki@tum.de

†e-mail: konstantinos.filippatos@zeiss.com

‡e-mail: abouzar.eslami@zeiss.com

§e-mail: navab@in.tum.de

2 METHODS

Our setup is shown in fig.1. It consists of an *OPMI LUMERA 700* microscope equipped with the *RESIGHT* fundus imaging system and an integrated *RESCAN 700* OCT engine connected to a *CALLISTO eye* assistance computer system (all from Carl Zeiss Meditec, Jena, Germany). A phantom eye was fixated under the optical pathway of the microscope. An artificial lens was attached to the phantom eye which optically mimicked a human eye lens. To simulate a realistic surgical setting, two 23-gauge sclera trocars were inserted into the phantom eye. A wide-angle 23-gauge endo-illumination probe was inserted into the phantom eye through the left trocar and the right trocar was used for insertion of the surgical instruments. The *OPMI LUMERA 700* microscope was focused on the retinal surface of the phantom eye while the *RESCAN 700* was configured to provide 2 real-time orthogonal OCT B-scans in form of a cross. The OCT B-scans were visualized both on the *CALLISTO eye* display and directly into the eyepiece of the microscope via HUD.

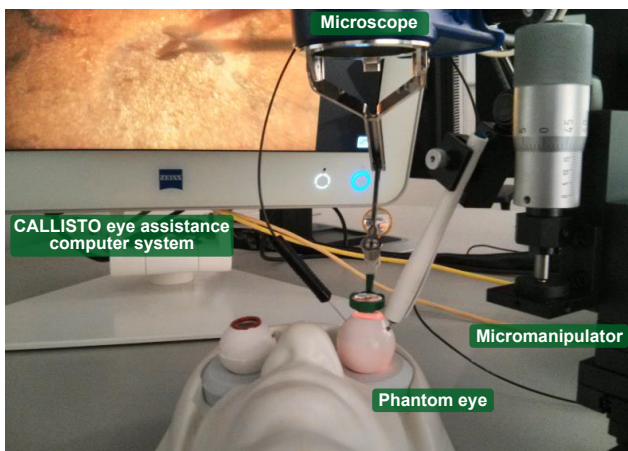


Figure 1: Our retinal surgery simulation setup. The surgical microscope is equipped with a fundus imaging system and a live OCT engine. The microscope is connected to an assistance computer system. A phantom eye is put under the optical pathway of the microscope. For evaluation purposes, the instruments are positioned using a micromanipulator.

Vitreoretinal instruments have tips with either one or two parts and are generally close to cylindrical in folded state for the ease of insertion. Instruments used in this preliminary work are considered of low geometrical complexity and include diamondized end-gripping vitreoretinal forceps, ILM end-gripping vitreoretinal forceps from various producers and posterior vitrectomy probe (Carl Zeiss Meditec, Jena, Germany). The common feature of these instruments is their cross-section being very close to either an ellipse or half-ellipses.

The basic principle behind our method of augmenting the surgeon's view of the OCT images with the instrument cross-section is illustrated in fig.3. Visualization of the instrument cross-section requires estimation of several instrument parameters such as its radius and orientation. These parameters are estimated based on the reflection of the instrument in the two perpendicular OCT images. For this purpose, the OCT scan position must be continuously kept at the instrument tip. Also the orientation of the scan must be such that one OCT B-scan is acquired perpendicular to the instrument and the other in the direction and over the instrument. Thus, the algorithm begins with the tracking of the instrument in the microscope image stream. For tracking the instrument in retinal images, we use the method described in detail

in [2] which provides the instrument tip and its orientation.

The second step is the detection of the retinal surface, the instrument reflections and their corresponding shadows in both OCT B-scans. Differentiation of the vitreous humor from the anatomical or artificial structures such as the retinal surface, the Internal Limiting Membrane (ILM) or the instrument reflections is done by thresholding the OCT images. The threshold value is adaptively defined based on statistical measures of each B-scan. This simple yet effective method has been used and evaluated in automatic segmentation of structures in OCT images in [1]. As a later step, morphological filtering is applied to eliminate thin vitreous membranes detected in the OCT images. Then the topmost surface is segmented and considered as the retinal surface. Scanning from left to right, any vertical jump and drop in this surface layer is detected and considered as the beginning and the end of an instrument reflection respectively. To avoid misdetection of anatomical features of retina as a reflection caused by a surgical instrument, only reflections with no visible structures below are confirmed as instrument reflections (fig.2b). For estimation and visualization of the cross-section, the instrument tip point in the OCT along the instrument and the topmost point or the mean of the topmost points of the instrument reflection in the OCT perpendicular to the instrument is extracted.

A cylindrical surgical instrument has a rectangular and an elliptical cross-section along its shaft and perpendicular to its shaft respectively. Augmenting both OCT B-scans with the cross-section of the instrument requires 5 parameters to estimate. The ellipse parameters are the center point (C_x, C_y), the major and minor axes (a, b) and the orientation angle (ϕ). The rectangle parameters are the top-left point (T_x, T_y), the sides (b, l) and the orientation angle (θ) as seen in fig.4.

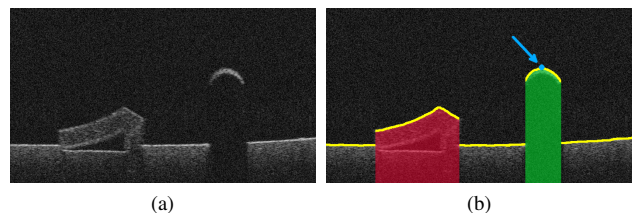


Figure 2: (a) A posterior segment OCT B-scan of a phantom eye featuring instrument shadowing and an abnormality on the retinal surface. (b) Detected features in the sample OCT image. Cuts in the topmost surface (yellow) are considered as instrument reflection candidates (red and green regions), but only reflections with no visible structures underneath get confirmed (green). The peak point of the instrument reflection (blue) is also detected.

The tracking of the instrument in the microscopic view guarantees one OCT image to be along the instrument shaft and the other perpendicular to that. Hence, the ellipse orientation angle (ϕ) is always zero and the orientation angle of the rectangle (θ) is the instrument orientation angle which can be estimated based on the slope of the instrument reflection in the OCT image along the instrument. Moreover the width of the instrument shadow in the perpendicular OCT equals the diameter of the instrument ($2r$). Which quickly gives the shorter side of the rectangular cross-section and the elliptical cross-section minor axis (b). Based on the cylindric section formulation, the following holds:

$$b = 2r, \quad a = 2r \sec \theta \quad (1)$$

The top-left point of the rectangular cross-section (T) could be set to the instrument tip point detected in the OCT over the instrument. To estimate the center point of the ellipse, the detected peak point

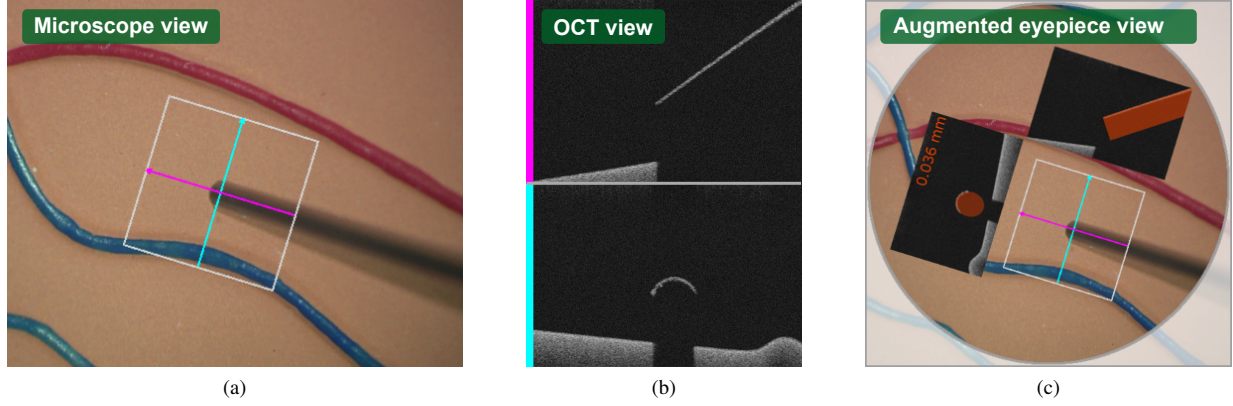


Figure 3: General instrument cross-section estimation scheme. (a) Tip of the instrument and its orientation is continuously detected in the microscopic view. (b) Two real-time OCT scans are constantly acquired over the instrument and perpendicular to the instrument at the instrument tip. Estimation of the instrument cross-sectional information is performed based on the instrument reflections in the two OCT scans. (c) The cross-sectional information is augmented into the OCT images and are directly put into the eyepiece of the microscope.

(P) of the instrument reflection in the OCT perpendicular to the instrument can be used as follows:

$$\begin{aligned} C_x &= P_x \\ C_y &= P_y + \frac{a}{2} \end{aligned} \quad (2)$$

Finally, since the OCT scans are centered on the instrument tip, the instrument is generally considered to be extended towards outside of the longer side of the rectangle. Thus the longer side of the rectangular cross-section (l) is set such that the rectangle is extended to the edge of the OCT image in both top and right edges.

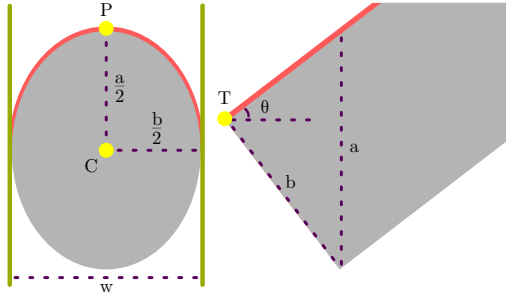


Figure 4: Cross-sections of a cylindrical instrument held at θ degrees. The upper red segments are the instrument reflections visible in OCT images, P and w are the instrument reflection peak point and shadow width in the perpendicular OCT image. The parameters to estimate are the instrument angle (θ), the ellipse axes (a , b), the ellipse center (C) and the rectangle top-left point (T).

Estimation of the cross-section in instruments with two-part tips (e.g. forceps) in the perpendicular OCT needs further calculations. Such instruments in their most basic form have cylindrical shafts, but cylindrical tips cut into halves along the axis of the shaft. Hence, the cross-sections to estimate in the OCT perpendicular to the instrument are half-ellipses. The instrument tracking provides the projection of the two parts of the tip on the instrument centerline as the instrument tip. Thus the instrument casts one shadow in one OCT scan which is treated the same as before to estimate the instrument slope and two shadows in the other OCT image. Although all the parameters of both half-elliptical cross-sections

are the same, to avoid propagation of the estimation error, each shadow is considered independent from the other. By doing so, one pair of independent parameters is estimated for the half-elliptical cross-sections (fig.5). This consideration guarantees less estimation error in case of misalignment of the OCT acquisition direction and the instrument caused by errors in instrument tracking.

In contrast to instruments with single-part tips (e.g. vitrectomy probe), a pair of forceps can also be tilted along the shaft axis. This instrument tilt angle (ϕ) must be taken into account for accurate cross-section estimation. The instrument tilt angle can be determined using the difference in the position of the two instrument reflection topmost points in the OCT image. This estimation of the instrument tilt is accurate since the OCT image is acquired perpendicular to the instrument shaft. The estimation of the axes of the ellipses is done with further considerations. The ellipses are now rotated by ϕ degrees. Moreover, since only half of the elliptical cross-section actually casts a shadow in the OCT image, the shadow width of each tip is extended to a value which would be covered if the tip was fully cylindrical. The concept is illustrated in fig.5. The width of each of the elliptical cross-sections axis-aligned bounding-box is relative to the ellipse axes. If both tips of the instrument were full cylinders, the radius of each one could be defined as:

$$\begin{aligned} w_i + e_i &= \sqrt{a_i^2 \sin^2 \phi + b_i^2 \cos^2 \phi} \\ b_i &= 2r_i \\ a_i &= 2r_i \sec \theta, \end{aligned} \quad i = 1, 2 \quad (3)$$

where i is the tip index. As illustrated in fig.5, the extended shadow length ($w_i + e_i$) can be estimated based on each ellipse semi-major axis and the ellipse rotation angle:

$$\begin{aligned} w_i + e_i &= 2(e_i + x_i) \\ x_i &= \frac{a_i}{2} \sin \phi, \end{aligned} \quad i = 1, 2 \quad (4)$$

By substituting $w_i + e_i$ from equation 4 into equation 3, the radius of each hypothetical cylindrical tip can be derived as follows:

$$r_i = \frac{w_i}{\sqrt{\frac{\sin^2 \phi}{\cos^2 \theta} + \cos^2 \phi + \frac{\sin \phi}{\cos \theta}}}, \quad i = 1, 2 \quad (5)$$

which immediately gives the axes of the ellipses. The ellipses are then cut into halves according to the tilt of the instrument. Finally,

each ellipse center point is defined as:

$$\begin{aligned} C_{ix} &= S_{ix} + \frac{w_i + e_i}{2} \\ C_{iy} &= P_{iy} + \frac{1}{2} \sqrt{a_i^2 \cos^2 \phi + b_i^2 \sin^2 \phi}, \quad i = 1, 2 \end{aligned} \quad (6)$$

in which P_i is the detected peak point. S_{ix} is the start of the occurrence of the i^{th} shadow in the x-axis in the perpendicular OCT. In other words, S_{ix} is the x element of the leftmost points of instrument reflections in the perpendicular OCT.

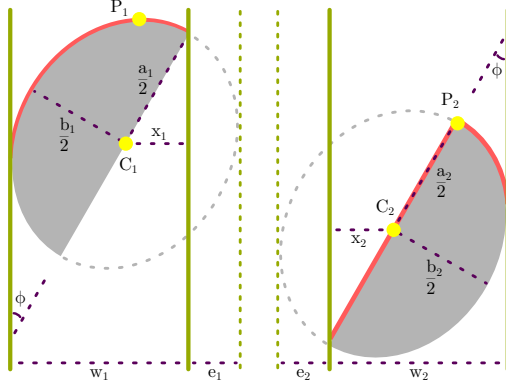


Figure 5: Cross-sections of a cylindrical instrument with a two-part tip held at θ degrees in the perpendicular OCT. The upper red segments are the instrument reflections visible in the OCT image. Estimation of the half-elliptical cross-sections, in excess of the parameters in the case of instruments with single-part tips, requires the extended shadow ($w_i + e_i$) and the instrument tilt angle (ϕ).

In either case of instruments with single-part tips or instruments with two-part tips, an estimation of the distance between the instrument tip and the underlying tissue is presented to the surgeon in real-time. For the estimation of the distance between the instrument tip and the retinal surface, the bottommost point of the estimated cross-section is needed. This point is straightforwardly determined based on the instrument reflection topmost point and the height of the axis-aligned bounding box of the estimated cross-section ellipse or half-ellipse. The difference between the mean of the retinal surface height detected immediately before and after the shadow region and the cross-section bottommost point is the desired distance to report. Since the pixel size of the OCT device is known, the distance in pixels is converted to the actual distance and is reported with micrometer resolution.

The augmentation of the surgeon's view is done via overlaying the estimated cross-sections and the estimated distance between the instrument tip and retina over the OCT images acquired at the instrument tip. Since concentration of the surgeon on the distance value is not feasible during surgery, a color coding mechanism is employed to facilitate the presentation of the estimated distance. The color of the instrument cross-sections are chosen from green to red spectrum based on the distance between the instrument and the retinal surface. Green represents $1mm$ or more and red is for $0.2mm$ or less. Also, the cross-sections are shown with less opacity if they are closer than $0.3mm$ to retina to avoid deviating the focus of the surgeon from the structure over retina which is under manipulation. These values are determined based on ex vivo experiments on pig eyes and geometrical footprints of the most typical vitreoretinal instruments used in the most common posterior manipulations such as ERM peeling and Vitrectomy.

The final synthesized image consists of a cross indicating the position of the two OCT scans and the augmented OCT images

(fig.3c). The OCT images are put at the top and left side of the cross if the instrument enters the scene from bottom right and at the top and right side if the instrument enters from bottom left. The synthesized image is then displayed in the HUD system which is optically coupled into the field-of-view (FOV) of one microscope ocular lens. Since the HUD is a half-mirror, the image is overlaid into the microscopic view. The HUD system of the microscope is internally registered to the scene under view. Thus, by providing the synthesized images in the same pixel size of the microscope, the overlay is correctly registered to the microscopic scene. An intraoperative OCT device requires thorough calibration between the OCT acquisition engine and the microscope. The HUD is also calibrated to the microscope FOV. The proposed method requires no further calibration. The instrument cross-section estimation and the augmentation is performed in real-time. Hence, the surgeon constantly gets feedback of the performed maneuvers.

3 RESULTS

The method is successfully employed to augment the OCT image stream of the described setup with the extra cross-sectional information (fig.6). The OCT B-scans used in our experiments are 8-bit, 1024×1024 pixels representing $3mm$ in width and $2mm$ in depth. The microscopic images used for instrument tracking are 24-bit, 720×540 pixels representing $8mm$ in width and $6mm$ in height. The microscope images along with the OCT B-scans are acquired at the rate of 25 frames per second. The computation and memory requirements of the developed algorithm are far above real-time limits. Although the method is intended to be an assistive tool in posterior ophthalmic procedures, tests in the anterior setup show the same overall results in terms of user experience and performance. A video demonstration of the proposed method is provided as supplementary material.

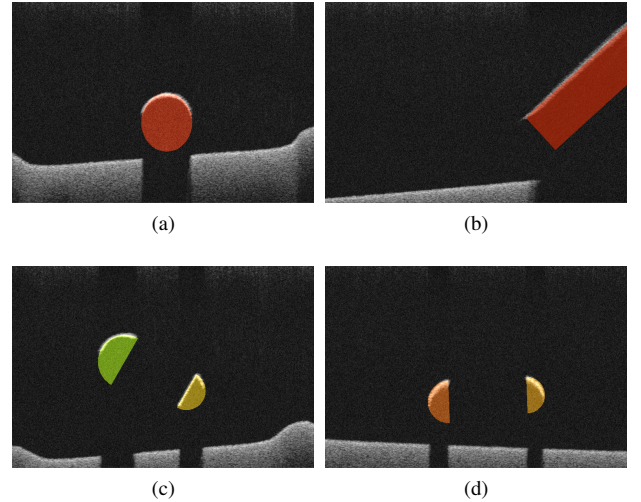
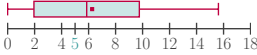
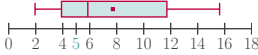




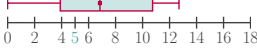













Figure 6: Examples of augmented OCT images in a simulated setup. (a) is augmented perpendicular OCT image of a vitreoretinal probe, (b) is augmented parallel OCT image of a diamondized forceps and (c) and (d) are augmented perpendicular OCT images of an ILM end-gripping forceps. The color of the cross-sections shifts towards red as the instruments get closer to the retinal surface.

To evaluate the accuracy of the proposed method, a relative measurement approach was applied in a simulated posterior setup. The detection accuracy of the instrument reflection topmost point in the perpendicular OCT as well as the estimation accuracy of the distance between the instrument tip and the

Table 1: Instrument Reflection Topmost Point Detection and Instrument-Retina Distance Estimation Accuracy

Instrument	Real movement in X and Z [μm]	Trial frames	Estimated topmost point movement in X [μm]	Estimated topmost point movement in Z [μm]	Estimated distance change [μm]
Posterior vitrectomy probe	5	82			
ILM end-gripping forceps*	5	394			
Diamonized forceps*	5	181			
Posterior vitrectomy probe	10	122			
ILM end-gripping forceps*	10	70			
Diamonized forceps*	10	173			

*For the forceps the mean of the estimated values for the two parts of the tip are considered.

retinal surface was evaluated using a 3-axes *HS-6* manual micromanipulator (Märzhäuser Wetzlar, Wetzlar, Germany). The employed micromanipulator has a resolution of 5 micrometers in each axis. In different trials, a 25-gauge posterior vitrectomy probe and two different types of 23-gauge vitreoretinal forceps were attached to the manipulator. The manipulator was positioned such that one axis of the manipulator was in the OCT depth direction and the other two axes in the height and width orientations of the microscope image plane. To avoid any interference in the movement of the instruments, instead of a trocar, a larger hole was created in the sclera region of the phantom eye. By accurately changing the position of the instrument in the orientation of the OCT width and depth, the relative change in the topmost point position detection and the distance to retina estimation was observed. For each instrument, a multitude of different trials at different locations with different distances between the instrument tip and retina were performed to suppress any effect caused by varying reflectivity of the phantom eye or the instruments. At each trial, several OCT frames were grabbed for evaluation. Also, instead of the instrument tracking algorithm, the position and orientation of the OCT scans were manually set according to the instrument to avoid the effect of the tracking error.

The evaluation results are presented in table 1. Each row of the table is representing the combination of a particular instrument and a fixed movement of 0.005mm or 0.01mm of the manipulator in the orientation of the OCT width and depth. The estimated topmost point movement and the estimated change in the distance between the instrument and the retinal surface is presented using box-and-whisker plots. In all of the plots, the whiskers are showing the minimum and maximum estimated change while the start and the end of the box are the first and third quartiles. The band and the dot inside the box are the median and mean of the estimated change respectively. The actual value against which the estimation should be compared is highlighted in blue on the horizontal axis of the plots. For the case of forceps, the mean of the estimated values for the two parts of the tip are plotted. The quantitative evaluation of the proposed AR solution shows that the maximum error in the estimation of the distance to retina is 9.76 micrometers which is the equivalent of 5 pixels in the OCT images of the test dataset.

Errors in detection of the topmost point induce error in estimation of the distance to retina. This is noticeable particularly in case of the posterior vitrectomy probe where a wide interquartile range in estimation of the topmost point movement leads to a wide interquartile range in the estimated distance change. In general, the more non-uniform the reflection from the instrument surface is, the wider the range between the minimum and maximum whiskers get. Hence, the observed wide minimum to maximum range is caused by variant reflections of the instrument in different OCT scans. In case of instruments with two-part tips, when the instrument is in the folded state it is considered to be an instrument with a single-part tip. Although this modeling causes very little error on its own, the irregular reflection due to the complex shape causes errors in detection of the topmost point.

4 CONCLUSION

In this paper, we introduced a novel method for augmenting the surgeon's view of intraoperative OCT images in ophthalmic surgery with instrument cross-section. We demonstrated that the information provided via the reflectivity characteristic of metallic vitreoretinal instruments in intraoperative OCT imaging can be employed to provide the surgeon with additional information regarding his maneuvers. Although the proposed method is an initial work in this direction, it shows the vast range of its applications and has the potential to be used in real clinical settings. Injecting extra information to the OCT images extends the reach of augmented reality to a new limit. The experiments demonstrate the robustness and the potential of the current approach for usage both in anterior and posterior ophthalmic setups. In [14], Gupta et al. have demonstrated that the majority of retinal surgery is performed without the surgeon being able to feel instrument-tissue interactions since most of the manipulations are below the human tactile sensation threshold. Hence, an estimation of the distance of the instrument tip to retina is valuable to avoid unnecessary touch of the delicate retinal tissue and the proposed AR paradigm is a suitable platform for providing this additional information. Also, the same study indicates that movements below tens of micrometers are believed to be below the limit of human positional ability. Thus, the proposed medical augmented reality method can be considered

as an assistive intraoperative tool considering its maximum error in estimation of the instrument to retina distance.

It is evident from the results that a robust augmentation of the parallel OCT is challenging in some cases due to the irregular shape of the instrument reflection. Hence, future work will direct towards extending the current approach for challenging instrument reflections and instruments with more complex geometries such as scissors. Having the 3D model of the instrument as prior knowledge would be one way to deal with instruments with complex shapes or augmenting the parallel OCT more smoothly. Also removing the reliability of the procedure on instrument tracking could be an applicable extension to the method. This would be particularly beneficial when the OCT is needed to be fixed on a specific location. Finally, design and application of a more sophisticated evaluation process to assess the accuracy of the estimated cross-section parameters such as the estimated radius of the instrument is of great importance. Instruments with known geometrical parameters at every location of the tip are required for such a task. A realistic clinical test to get feedback from surgeons and evaluation of the method in more realistic scenarios is also of great benefit.

ACKNOWLEDGEMENTS

The authors would like to thank Carl Zeiss Meditec AG for providing the opportunity to use their ophthalmic imaging devices and surgical instruments and Dr. Corinna Maier-Matic and Falk Hartwig for their support.

REFERENCES

- [1] C. Ahlers, C. Simader, W. Geitzenauer, G. Stock, P. Stetson, S. Dastmalchi, and U. Schmidt-Erfurth. Automatic segmentation in three-dimensional analysis of fibrovascular pigmentepithelial detachment using high-definition optical coherence tomography. *British Journal of Ophthalmology*, 92(2):197–203, 2008.
- [2] M. Alsheakhali, M. yigitsoy, A. Eslami, and N. Navab. Surgical tool detection and tracking in retinal microsurgery. In *Proceedings of SPIE Medical Imaging*. SPIE, 2015.
- [3] J. W. Berger and D. S. Shin. Computer-vision-enabled augmented reality fundus biomicroscopy. *Ophthalmology*, 106(10), 1999.
- [4] S. Binder, C. I. Falkner-Radler, C. Hauger, H. Matz, and C. Glittenberg. Feasibility of intrasurgical spectral-domain optical coherence tomography. *Retina*, 31(7):1332–1336, 2011.
- [5] R. A. Costa, M. Skaf, L. A. M. Jr., D. Calucci, J. A. Cardillo, J. C. Castro, D. Huang, and M. Wojtkowski. Retinal assessment using optical coherence tomography. *Progress in Retinal and Eye Research*, 25(3):325 – 353, 2006.
- [6] W. Drexler and J. G. Fujimoto. State-of-the-art retinal optical coherence tomography. *Progress in Retinal and Eye Research*, 27(1):45 – 88, 2008.
- [7] P. Edwards, A. King, J. Maurer, C.R., D. De Cunha, D. Hawkes, D. Hill, R. Gaston, M. Fenlon, A. Juszczak, A. Strong, C. Chandler, and M. Gleeson. Design and evaluation of a system for microscope-assisted guided interventions (magi). *Medical Imaging, IEEE Transactions on*, 19(11):1082–1093, Nov 2000.
- [8] J. P. Ehlers, W. J. Dupps, P. K. Kaiser, J. Goshe, R. P. Singh, D. Petkovsek, and S. K. Srivastava. The prospective intraoperative and perioperative ophthalmic imaging with optical coherence tomography (pioneer) study: 2-year results. *American Journal of Ophthalmology*, July 2014.
- [9] J. P. Ehlers, P. K. Kaiser, and S. K. Srivastava. Intraoperative optical coherence tomography using the rescana 700: preliminary results from the discover study. *British journal of Ophthalmology*, 98(10):1329–1332, 2014.
- [10] J. P. Ehlers, S. K. Srivastava, D. Feiler, A. I. Noonan, A. M. Rollins, and Y. K. Tao. Integrative advances for oct-guided ophthalmic surgery and intraoperative oct: Microscope integration, surgical instrumentation, and heads-up display surgeon feedback. *PLoS ONE*, 9(8):e105224, 08 2014.
- [11] J. P. Ehlers, Y. K. Tao, S. Farsiu, R. Maldonado, J. A. Izatt, and C. A. Toth. Integration of a spectral domain optical coherence tomography system into a surgical microscope for intraoperative imaging. *Investigative Ophthalmology & Visual Science*, 52(6):3153–3159, 2011.
- [12] J. P. Ehlers, Y. K. Tao, and S. K. Srivastava. The value of intraoperative optical coherence tomography imaging in vitreoretinal surgery. *Current Opinion in Ophthalmology*, 25(3):221–227, 2014.
- [13] I. Fleming, S. Voros, B. Vagvolgyi, Z. Pezzementi, J. Handa, R. Taylor, and G. Hager. Intraoperative visualization of anatomical targets in retinal surgery. In *Applications of Computer Vision, 2008. WACV 2008. IEEE Workshop on*, pages 1–6, Jan 2008.
- [14] P. K. Gupta, P. S. Jensen, and J. de Juan, Eugene. Surgical forces and tactile perception during retinal microsurgery. In C. Taylor and A. Colchester, editors, *Medical Image Computing and Computer-Assisted Intervention MICCAI99*, volume 1679 of *Lecture Notes in Computer Science*, pages 1218–1225. Springer Berlin Heidelberg, 1999.
- [15] P. Hahn, J. Migacz, R. O’Connell, R. S. Maldonado, J. A. Izatt, and C. A. Toth. The use of optical coherence tomography in intraoperative ophthalmic imaging. *Ophthalmic surgery, lasers & imaging : the official journal of the International Society for Imaging in the Eye*, 42 Suppl:S8594, July 2011.
- [16] N. Hirschschall, S. Norrby, M. Weber, S. Maedel, S. Amir-Asgari, and O. Findl. Using continuous intraoperative optical coherence tomography measurements of the aphakic eye for intraocular lens power calculation. *British journal of Ophthalmology*, 2014.
- [17] N. Navab, T. Blum, L. Wang, A. Okur, and T. Wendler. First deployments of augmented reality in operating rooms. *Computer*, 45(7):48–55, July 2012.
- [18] R. Richa, M. Balicki, R. Sznitman, E. Meisner, R. Taylor, and G. Hager. Vision-based proximity detection in retinal surgery. *Biomedical Engineering, IEEE Transactions on*, 59(8):2291–2301, Aug 2012.
- [19] T. Sielhorst, M. Feuerstein, and N. Navab. Advanced medical displays: A literature review of augmented reality. *Display Technology, Journal of*, 4(4):451–467, Dec 2008.
- [20] Y. K. Tao, S. K. Srivastava, and J. P. Ehlers. Microscope-integrated intraoperative oct with electrically tunable focus and heads-up display for imaging of ophthalmic surgical maneuvers. *Biomedical optics express*, 5(6):18771885, June 2014.